JOURNAL OF AIRCRAFT
Vol. 35, No. 5, September–October 1998

Effects of Ballistic Damage on the Aerodynamics of Helicopter Rotor Airfoils

Keith W. Robinson* and J. Gordon Leishman†
University of Maryland, College Park, Maryland 20742-3015

Experiments were conducted to estimate the effects of ballistic damage on the aerodynamics of helicopter rotor airfoil sections. The lift, pitching moment, and drag were measured on nominally two-dimensional blade specimens with representative prescribed and actual ballistic damage. The measurements were made at chord Reynolds numbers between 1×10^6 and 3×10^6 and Mach numbers up to 0.28. Force balance measurements were complemented by chordwise and spanwise pressure measurements to assess the three-dimensional nature of damage on the aerodynamics. The quantitative data were supplemented by surface oil-flow visualization. Generally, it was found that ballistic damage degraded the aerodynamic performance of the blade specimens, with a reduction in lift accompanied by significant increase in drag and change in the center of pressure. However, in some cases significant damage produced surprisingly mild effects. The results are useful in helping to model and assess the overall vulnerability of helicopters to ballistic damage.

Introduction

THE vulnerability of the main and tail rotor systems to ballistic damage is an important design consideration for military helicopters. Ballistic damage is most likely realized in a mission where full combat capability would be needed. Because helicopters fly lower and slower than most fixed-wing aircraft in these situations, they are generally more vulnerable to ballistic damage. Also, helicopters have a much lower degree of system redundancy than fixed-wing aircraft because they depend entirely on the rotor system(s) for lift generation, propulsion, and control. Therefore, damage inflicted to the rotor system(s) is less likely to have survivable consequences.

Like all modern military aircraft, helicopters have stringent design requirements regarding vulnerability.[1] Increased emphasis on the survivability of aircraft was instigated by the Joint Coordinating Group on Aircraft Survivability.[2] Outgrowths of this effort have been the Joint Live Fire (JLF) test program and, more recently, the Target Interactions Lethality Vulnerability program.[3] Live-fire testing can uncover vulnerable airframe components and systems unforeseen by designers and, therefore, can help improve survivability. Consequently, a major benefit of the JLF program has been an improved understanding of the design of ballistically tolerant flight systems and structures. In addition to live-fire tests, numerical models of the effects of ballistic damage are becoming increasingly essential for providing insights into the various tradeoffs during the design process.[4,5]

Modern composite materials give a high-level damage tolerance to helicopter rotor blades in terms of structural soundness and fatigue strength. However, ballistic damage can also affect the performance (thrust and power), vibration levels, and aeroelasticity of the rotor system. These effects are currently poorly understood, but experience dictates that they contribute significantly to the capability (and vulnerability) of the aircraft even if structural soundness can be maintained. Unfortunately, most of these effects and their interdependencies are difficult to predict and assess. For example, damage effects on the blade aerodynamics will be a function of several interrelated parameters, including the damaged location on the blade (chordwise and spanwise), physical nature, and extent of damage. At a minimum a damaged area on the blade may be expected to decrease the blade section lift and to increase drag. This will result in increased rotor power requirements, the possibilities of premature blade stall, high control forces, and increased vibration levels. Even a minor aerodynamic degradation on the rotor may incur a much higher fuel burn and may seriously limit the ability of the helicopter to complete its assigned mission. A quantitative understanding of the aerodynamic effects of ballistic damage on the rotor system is, therefore, essential to accurately assess the capability and vulnerability of the helicopter in a combat situation.

The subject of ballistic damage as it affects the aerodynamics and aeroelasticity of lifting surfaces is not new. Some of the earliest recorded tests on the aerodynamic effects of ballistic damage were performed by the NACA in 1936, which examined the effects of machine gun and cannon fire on the lift and drag properties of fabric-covered aircraft wings.[6] In the 1950s, aeroelastic and flutter studies of aircraft wings with structural damage were conducted by Biot and Arnold.[7] Also during the 1950s, systematic experimental investigations were carried out at the Cornell Aeronautical Laboratory to study the aerodynamic characteristics of fixed wings with ballistic damage.[8] These approaches are highly empirical, but included measurements of the drag increase incurred by different damaged configurations. This formed the basis for later studies by Chang and Stearman[9] into the aeroelastic integrity of a ballistically damaged wing. A follow-on study was later performed by Westkaemper and Chandrasekharan.[10]

It is very difficult to quantify ballistic damage effects on the aerodynamic and aeroelastic characteristics of helicopter rotor blades. This is partly because of the three-dimensional and time-varying flow environment in which the blades operate. Eastman[11] has assessed the effects on a UH-60 main rotor blade subjected to ballistic damage. Because no experimental data on the blade airloads were available, the effects of ballistic damage on the airfoil section characteristics were estimated based on hypothesized changes to chordwise pressure distributions. Recognizing the limitations of this approach, Eastman

Received June 8, 1997; revision received Dec. 21, 1997; accepted for publication March 24, 1998.

*Major, U.S. Army, Department of Aerospace Engineering, Glenn L. Martin Institute of Technology; currently at the Office of the Assistant Secretary of the Army—Research, Development and Acquisition, The Pentagon, Washington, DC.

†Associate Professor, Department of Aerospace Engineering, Glenn L. Martin Institute of Technology. Senior Member AIAA.

recommended that wind-tunnel measurements with damaged blade sections be performed for use in any future vulnerability analysis.

Preliminary experimental measurements of the aerodynamic characteristics of a helicopter blade section with typical but prescribed ballistic damage was conducted by Leishman.[12] The results showed the expected degradation in the aerodynamics and provided new insight into the flow effects caused by damage. However, it was clear from the results of Ref. 12 that a more systematic study into the effects of damage size, chordwise location, and nature of damage was imperative to gain an improved understanding of the problem and, also for the development and/or improvement of mathematical models representing these degraded aerodynamic effects in helicopter vulnerability analyses. It is to this end that the present work is directed.

Experiment Description

Aerodynamic measurements were conducted on a series of helicopter blade specimens that were taken from actual U.S. Army helicopter rotor blades representative of currently fielded systems. The experiments were conducted in the Glenn L. Martin (GLM) wind tunnel at the University of Maryland, the tests being made using a standard two-dimensional insert placed within the working section. This insert consisted of floor to ceiling false walls, with the blade specimen spanning these two walls in a manner similar to that described by Rae and Pope.[13] An extended flat center section on the walls contained two floating circular disks with labyrinth seals to which the blade specimens were mounted. The disks were rotated by a pitch-drive mechanism that was composed of a ring gear driven by a servomotor through a transmission. This arrangement enabled the blade specimens to be rotated a full 360 deg. An angular displacement transducer was used to determine the geometric angle of attack of the blade section to within ± 0.1 deg.

The entire blade-section support structure and pitch-change mechanism was mounted to a six-component yoke balance system, which was used to find the average (nominally two-dimensional) airloads on each blade specimen. In the case of the undamaged specimen, the technique for measuring and extrapolating to two-dimensional airfoil characteristics in this manner has been well validated by comparisons with integrated sectional pressures. In the case of the damaged specimens, the approach used here was to estimate the effects of damage on the average (nominally two-dimensional) airloads over a section of the blade that can be considered representative of a blade element. In practice, the measured results can be implemented semiempirically in a blade-element analysis of the rotor in terms of zones of effectivity, although the details of this approach are beyond the scope of the present article.

Blade Specimens

The blade sections used for this work were composed of the SC1095 and SC1095-R8 airfoils, which are typical of advanced helicopter rotor sections. The airfoil section coordinates are tabulated in Ref. 14. The blades had a pretwist angle (leading-edge down from root to tip), so that the angle of attack was referenced to the midspan of the section. Based on balance measurements (roll-moment) and flow visualization, the mild amount of built-in twist was found to produce little in the way of asymmetric loading over the span. Before testing all specimens were refurbished to an aerodynamically smooth contour typical of new factory blades.

Ten different blade specimens were tested (Table 1 and Fig. 1), with two reference undamaged blade specimens and eight damaged blade configurations. Further details of the damaged specimens are documented in Ref. 15. Generally, the tests on the various blade sections were combined as specimens sharing the same airfoil profile. Specimen 1 was an undamaged blade section used to establish the baseline characteristics of the SC1095 airfoil. This blade section was subsequently modified for testing as specimen 1A, where ballistic damage at the trailing edge was simulated by means of a plain circular hole of diameter 19.3% of chord ($0.193c$) located at the midspan and centered $0.75c$ downstream of the leading edge.

Table 1 Summary of undamaged and damaged blade specimens

Specimen	Airfoil	Damage
1	SC1095	Undamaged
1A	SC1095	TE circular hole
1B	SC1095	TE wedge
1C	SC1095	Actual ballistic damage
1D	SC1095	Undamaged, w/pressure taps
1E	SC1095	Midchord circular hole, w/pressure taps
2	SC1095-R8	Undamaged
2A	SC1095-R8	LE circular hole
2B	SC1095-R8	As 2A w/petalling
2C	SC1095-R8	TE circular hole

Specimen 1C was subjected to actual ballistic damage through which a representative projectile was fired. The location and nature of the damage was specified on the basis of live-fire tests conducted on spinning rotor blades. The resulting damage on this specimen consisted of a single main hole completely through the blade surrounded by several smaller holes, and with a large irregular area of damage in the trailing-edge region. Delamination of the blade skin along the composite skin ply angles produced an almost wedge-shaped damaged region. This damage configuration is detailed in Ref. 15.

The actual damage case was also used to define a simulated damaged case (1B) of the same approximate size and location of the actual ballistic damage. The intent here was to compare results to see if a more controlled simulated damage case could be considered representative of actual damage for ease in the modeling. Therefore, a wedge shape with a base of $0.674c$ and a height of $0.327c$ was cut from specimen 1A. The apex of the wedge was located $0.625c$ downstream of the leading edge, with the base of the cutout area located $0.048c$ upstream from the trailing edge.

For specimen 1E, damage was simulated by means of a circular hole $0.241c$ in diameter. This hole was cut at the midspan and was centered $0.60c$ downstream of the leading edge. Around the periphery of the hole, a $0.05c$ ring of the fiberglass skin was removed to expose the paper honeycomb interior structure of the blade. This blade section was also tested in its undamaged state as specimen 1D, which was another baseline specimen with an SC-1095 airfoil. Specimen 1D was identical to specimen 1, but both specimens 1D and 1E had static pressure taps installed.

Specimen 2 was used to establish the baseline characteristics for the SC1095-R8 airfoil. Ballistic damage for specimen 2A was simulated by means of a circular hole $0.193c$ in diameter. This hole was cut at midspan and centered $0.24c$ downstream of the leading edge. Of note here is that the hole in specimen 2A was cut through the center of the hollow metal spar on the blade. To simulate the petalling that often takes place when a projectile passes through metal, a ring of serrations approximately $0.024c$ high was attached around the circumference of the hole in specimen 2A (specimen 2B). While perhaps somewhat artificial, this gave a well-defined geometry for later analysis.

Oil-Flow Visualization

Flow visualization was performed on each blade configuration at various Reynolds numbers and angles of attack. An oil mixture consisting of mineral oil and dissolved titanium dioxide was applied to the upper and lower surfaces of each blade section. Oil was also applied on the adjoining left and right walls of the two-dimensional insert. The tunnel wind speed was quickly increased to the target wind speed, followed

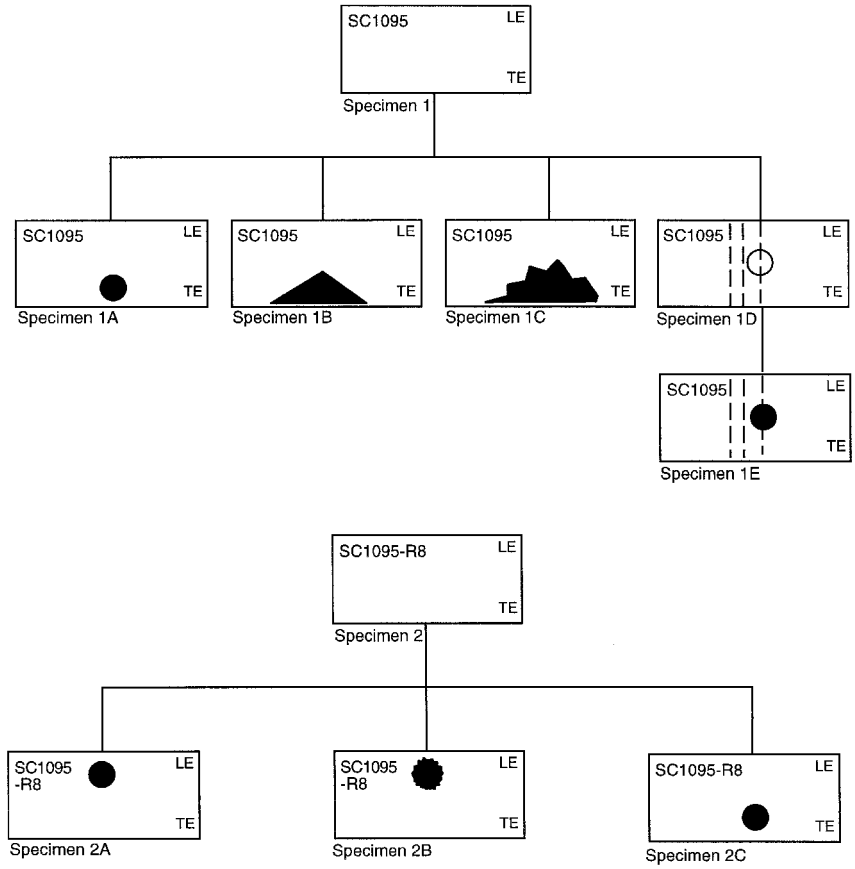

Fig. 1 Schematic showing blade specimens tested with type and pattern of damage.

by setting the angle of attack to the required value. When the flow pattern developed, a white deposit was left on the blade surface. The results were recorded on high-contrast black and white film.

Force Balance Measurements

Force balance measurements on each specimen were made at chord Reynolds numbers of 1×10^6, 2×10^6, and 3×10^6 (Mach numbers of approximately 0.08, 0.16, and 0.24, respectively). Only results for a Reynolds number of 2×10^6 are discussed in this article. Both the negative and positive angle-of-attack ranges were examined up through stall. Generally, tests were conducted over angles of attack ranging from -25 to 35 deg in steps of 1 deg or smaller. Smaller angle-of-attack increments (one-quarter of a degree) were taken near the point of maximum lift. For specimens 1D and 1E, additional tests were conducted at a Reynolds number of 1×10^6 over an angle-of-attack range of 360 deg.[15]

The lift, drag, and pitching moment were measured using standard computer-controlled data-acquisition techniques established for the GLM wind tunnel. Increasing angle-of-attack sweeps were made for all cases. Deadweight tares were obtained from balance measurements with each blade specimen with the wind off. Tares were obtained over the required range of angles of attack, and automatically subtracted from the measurements during the data-acquisition process. Balance loads were sampled up to 300 times at each angle of attack, and were ensemble-averaged on-line to maintain a prescribed tolerance and statistical accuracy. The data were obtained to a desired precision in each force and moment component based on an equation of the form

$$P = k\sigma/\sqrt{n} \tag{1}$$

where P is the target precision, σ is the standard deviation, n is the number of samples acquired, and k is a factor that is a function of the level of confidence and the number of samples. The force balance results were converted into sectional coefficients in the normal way. No wall corrections were applied to the measured data.

The dynamic pressure in the test section was measured indirectly as a pressure drop between the static pressure in the settling chamber and the average static pressure measured at a ring of orifices at the forward upstream end of the test section. The relationship between the pressure drop and the actual dynamic pressure in the two-dimensional insert was obtained by means of a calibration with a reference NASA pitot–static probe.

Static Pressure Measurements

Fifty-eight pressure taps (33 on the upper surface and 25 on the lower surface) were installed into blade specimens 1D/1E. The taps were concentrated at three spanwise stations, midspan (location no. 3), 23% of span to port of midspan (location no. 2), and 35.4% of span to port of midspan (location no. 1), when looking upstream. The detailed locations of the pressure taps are given in Ref. 15. Integration of these static pressure measurements allowed for a direct comparison between the strictly two-dimensional and the nominally two-dimensional (averaged) aerodynamic characteristics measured directly from the force balance system. The spanwise pressure measurements also allowed for a limited determination of three-dimensional flow effects produced by the damage regions on the specimen.

The pressure measurements were made using a multichannel data acquisition and control unit (DACU). The DACU contained 64 miniature quartz pressure transducers, analog multiplexers, and A/D converters. Fifty-eight static ports were used with the remaining six channels of the DACU being used for reference static and dynamic pressures. A miniature pneumatic valving system in the DACU permitted rapid on-line

Table 2 Summary of estimated errors in measured quantities

Parameter	Uncertainty
Lift L	± 0.1 lbf
Drag D	± 0.1 lbf
Moment M	± 0.5 ft-lb
Dynamic pressure q_∞	± 0.072 lb/ft^2
Blade section area A	± 0.065 ft^2

recalibration of the individual pressure sensors as the tests proceeded.

Experimental Accuracy

All of the balance loads were ensemble-averaged on-line to maintain a prescribed absolute tolerance and statistical accuracy. The error in the measurement of the aerodynamic coefficients is a function of the uncertainty in the measurements of lift, etc. The uncertainty W_{C_l} in the lift coefficient C_l is given by

$$W_{C_l} = \left[\left(\frac{\partial C_l}{\partial L} W_L \right)^2 + \left(\frac{\partial C_l}{\partial q_\infty} W_{q_\infty} \right)^2 + \left(\frac{\partial C_l}{\partial A} W_A \right)^2 \right]^{1/2} \quad (2)$$

where W_L, W_{q_∞}, and W_A are the errors in the measurement of the lift force, the freestream dynamic pressure, and the blade specimen area, respectively, as documented in Table 2. The preceding equation may be simplified to obtain the relative error in C_l, giving

$$\frac{W_{C_l}}{C_l} = \left[\left(\frac{W_L}{L} \right)^2 + \left(\frac{W_{q_\infty}}{q_\infty} \right)^2 + \left(\frac{W_A}{A} \right)^2 \right]^{1/2} \quad (3)$$

Similar equations can be derived to obtain the errors in the measurements of C_m and C_d. The estimated uncertainties in the lift coefficient were less than 2% for all angles of attack. The uncertainties in the moment coefficient were estimated to be 4% in the attached flow regime, and less than 2% in the poststall condition. The maximum uncertainty in the drag coefficent was estimated to be 6% at low angles of attack below stall and 2% in the poststall condition. There were exceptions to these estimated uncertainties when periodic flow separation (buffeting) occurred on the specimens at high angles of attack (above 30 deg). The estimated errors in the pressure coefficients were about ± 0.02.

Results and Discussion

Oil-Flow Visualization

Examples showing the effects of damage on the flow over the top surface of the blade specimens are shown in Fig. 2. Figure 2a shows results for the undamaged SC1095 airfoil at an angle of attack of 15 deg, just below stall. For these conditions the flow was found attached over about 60% of chord, but there was evidence of some trailing-edge flow separation. The separation front was found to be fairly uniform along the span, except at the airfoil/wall junctions, where there was some evidence of some three-dimensional flow. With further increases in angle of attack the trailing-edge separation front was found to move fairly quickly forward to the vicinity of the leading edge and the airfoil stalled by the trailing-edge separation mechanism.

Figure 2b shows the flow pattern obtained with specimen 1E at an angle of attack of 14 deg. Note that the simulated ballistic damage (a circular hole) caused flow separation at the upstream edge of the hole. This was found even at low angles of attack, where the increased separation produced a significant increase in drag (seen later in this paper). It can be seen from Fig. 2b that a pair of counter-rotating or mustache vortices were formed at the upstream edge of the damaged region, and

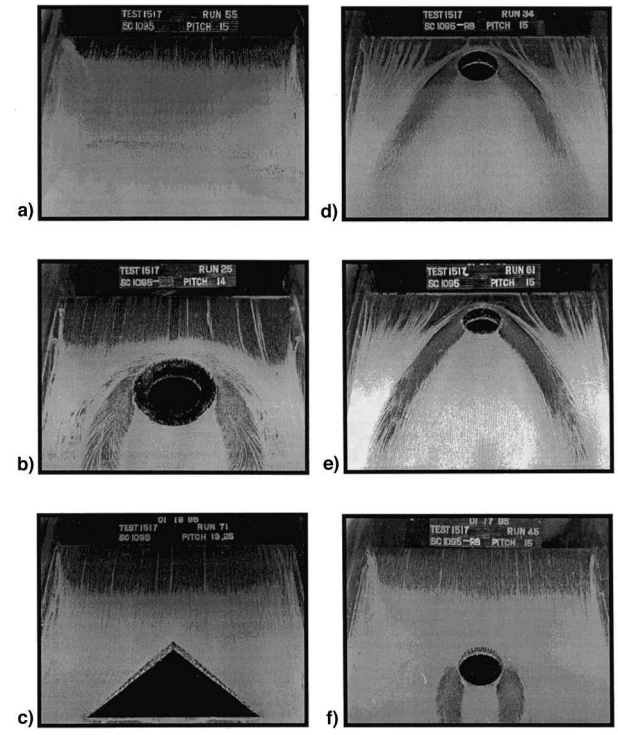

Fig. 2 Samples of oil-flow visualization on the blade sections: a) baseline SC1095 (specimen 1), b) specimen 1E, c) specimen 1B, d) specimen 2A, e) specimen 2B, and f) specimen 2C.

these trailed back across the chord. Away from the vicinity of the hole the flow separation point occurred near the trailing edge, which moved upstream with increasing angle of attack.

Figure 2c shows the flow pattern obtained with specimen 1B at an angle of attack of 13.25 deg. Although a substantial amount of lifting area was removed from trailing edge of the specimen, the overall flow pattern was relatively unchanged compared to the baseline (undamaged) specimen. However, flow separation was produced all along the upstream edges of the damaged region. This form of damage was found to cause stall to occur at essentially the same (or slightly higher) angle of attack compared to the undamaged section.

Figures 2d and 2e show the flow patterns obtained with specimens 2A and 2B at an angle of attack of 15 deg, which was close to maximum lift. In these cases, the damage was situated at the leading edge of the airfoil. Specimen 2B differed from 2A by the addition of serrations around the top periphery of the hole. In this case, there was clear evidence of substantial flow separation, with the formation of a pair of stable mustache vortices at the upstream leading edge of the hole. The serrations on specimen 2B did not substantially affect the flow, although immediately downstream of the hole the serrations produced a more energetic wake with stronger flow reversals on the airfoil surface. It was found that at lower angles of attack the vortices generated at the hole were weaker and affected less of the span, but for increasing angle of attack the region of flow separation quickly expanded over a larger part of the blade specimen.

Figure 2f shows the flow pattern obtained with specimen 2C (SC1095-R8 airfoil) at an angle of attack of 15 deg. This damage configuration is the same as that for specimen 1A (SC1095 airfoil). The flow patterns between both airfoils were found to be substantially similar, although specimen 2C produced somewhat less trailing-edge separation away from the vicinity of the damage. This was expected because the nose camber on the SC1095-R8 airfoil helps alleviate the leading-edge pressure gradients and delay the onset of trailing-edge separation to a higher angle of attack and to a higher value of lift coefficient.

In all of these flow visualization tests it was noted that a laminar separation bubble remained present throughout the entire range of angles of attack up through stall. This could be deduced from an accumulation of oil in a narrowband near the leading edge. As the angle of attack was increased, the separation bubble moved well forward onto the leading edge and became much narrower in a chordwise extent. The bubble was not found to directly participate in the stall mechanism for any of the specimens tested in this experiment, through bubble bursting nor by abrupt reseparation of the flow downstream of the bubble. In all cases the flow was found to separate from the trailing edge and move forward on the chord with increasing angle of attack.

Force and Moment Results

Undamaged Specimens

Comparisons were conducted between the baseline SC1095 and SC1095-R8 airfoil sections. Figure 3 shows results for a Reynolds number of 2×10^6. The SC1095-R8 airfoil has a modified nose shape with increased camber over that of the SC1095 and is designed to enhance maximum lift. This is confirmed in the measured results, where the -R8 airfoil showed about a 0.1 increase in maximum lift coefficient relative to the SC1095 airfoil. The pitching moment in the normal (positive) angle-of-attack range was close to the baseline SC1095 section; there was little or no change in the position of the aerodynamic center in the positive lift range, and the zero-lift moment was only slightly more nose down. The effect of the -R8 airfoil on the section drag also appeared to be minimal, with a very slight increase relative to the SC1095 airfoil.

Damaged Specimens

Results for each of the damaged specimens are presented individually and are compared to the respective undamaged specimens at a Reynolds number of 2×10^6. Further results comparing damaged specimens and also measurements at other Reynolds numbers are given in Refs. 13, 16, and 17.

Figure 4 shows results for specimen 1A (trailing-edge circular hole) vs the undamaged SC1095 specimen. For this specimen the aerodynamic effects of damage were relatively small, with only a slight change in the lift-curve slope and about a 0.1 decrease in maximum lift. The damage in the trailing-edge region caused the aerodynamic center to move slightly forward relative to the undamaged specimen. As expected, the damage produced higher drag in the low-angle-of-attack region, with an increase in zero-lift drag coefficient from a baseline of 0.011 to about 0.016. The rate of increase in drag with angle of attack, however, was relatively unaffected by the damage. Overall, the damage caused the maximum lift-to-drag ratio to decrease from 40 to about 28.

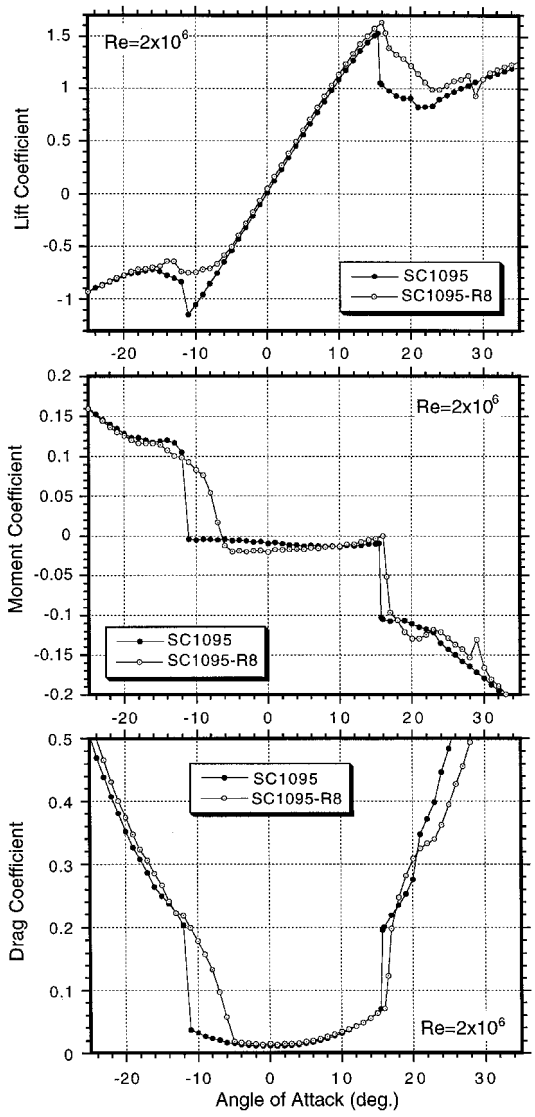

Fig. 3 Comparison of the lift, moment, and drag coefficients of the undamaged SC1095 and SC1095-R8 blade sections.

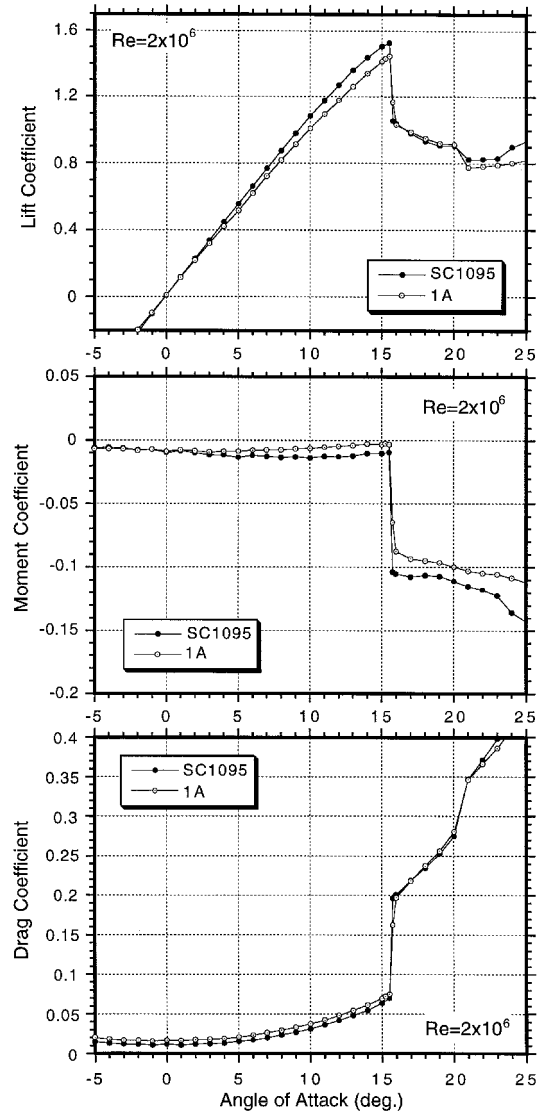

Fig. 4 Comparison of the lift, moment, and drag coefficients of specimen 1A (trailing-edge hole) vs the undamaged SC1095 section.

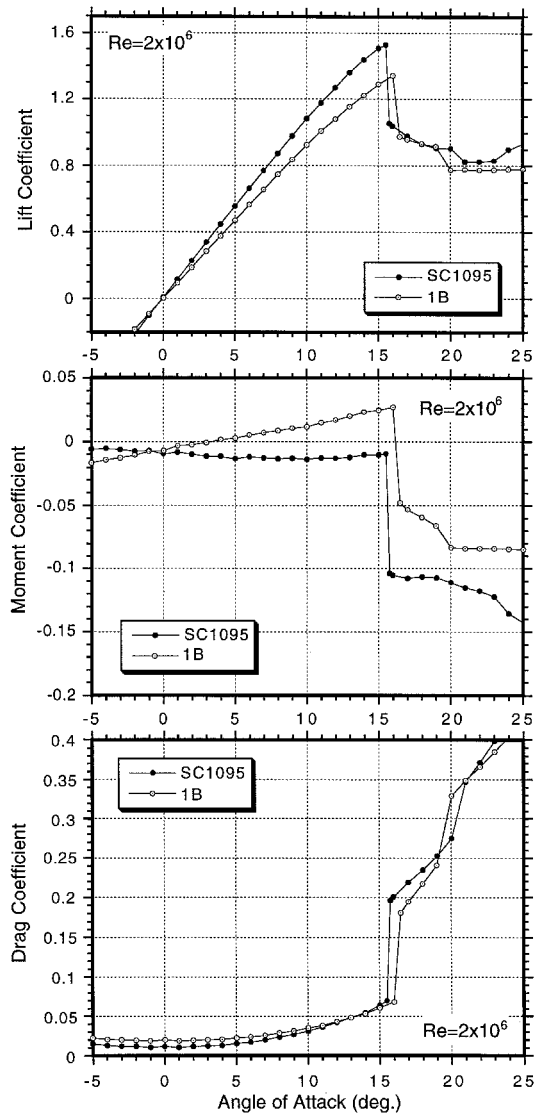

Fig. 5 Comparison of the lift, moment, and drag coefficients of specimen 1B (trailing-edge wedge hole) vs the undamaged SC1095 section.

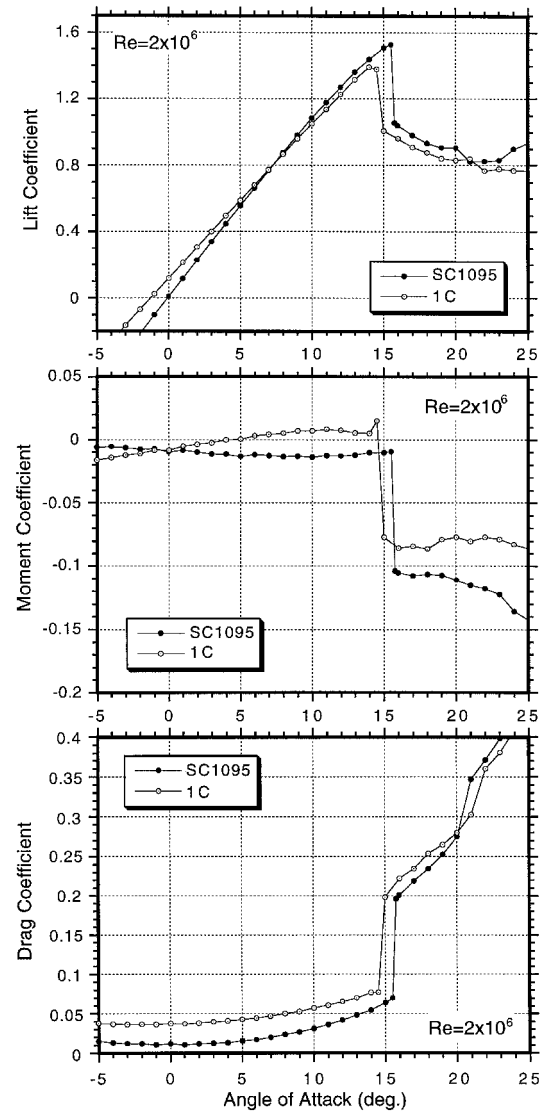

Fig. 6 Comparison of the lift, moment, and drag coefficients of specimen 1C (actual ballistic damage) vs the undamaged SC1095 section.

Figure 5 shows results for specimen 1B (trailing-edge, wedge-shaped damage) vs the undamaged SC1095 specimen. This case was selected to be representative of the actual damaged specimen (considered next). Here the effects of damage on the airloads showed a more notable decrease in lift-curve slope (about 10%) and a more significant decrease in maximum lift coefficient (about 0.2). Surprisingly, the damage in this case was found to increase the stall angle of attack from about 15.5 to 16.5 deg. There was also a larger forward movement of the aerodynamic center, which is symptomatic of a fixed chordwise point of flow separation and a loss of lifting area over the trailing edge. This form of damage caused a more measurable increase in the section drag by nearly a factor of 2 over the undamaged section in the low-angle-of-attack regime, but this difference decreased somewhat at higher angles of attack.

Figure 6 shows the results obtained for specimen 1C (actual ballistic damage) vs the undamaged SC1095 specimen. Here, the damage produced a decrease in lift-curve slope of about 10% and a decrease in maximum lift coefficient of about 0.2, which were almost the same as that found for specimen 1B. However, in this case there was also a reduction in the zero-lift angle by just over 1 deg, which makes the differences in the lift curves less pronounced compared to specimen 1B. This effect on the zero-lift angle of attack was likely because of damage incurred at the trailing-edge bond line of the blade that was split along its length compared to specimen 1B. Nevertheless, the maximum lift coefficient was reduced only by about 0.2, despite the relatively large amount of damage. This form of damage caused the c.p. to migrate forward, although a little less so than for specimen 1B. The pitching moment behavior was found to be much more nonlinear beyond 9- or 10-deg angle of attack, which was obviously a result of the more complicated separated flow structure that existed for the actual damaged specimen compared to specimen 1B. In this case, as expected, the drag was much higher than for the undamaged specimen or for specimen 1B because of the delamination of the skin plys. The zero-lift drag coefficient was determined to be about 0.037, which was nearly four times the value obtained with the undamaged specimen.

Figure 7 shows the results obtained for specimen 1E (circular hole near midchord) compared to the undamaged SC1095 section. A ring of the composite skin was removed from the periphery of the hole to expose the internal honeycomb structure. This type of blade damage where skin is removed is also typical of that caused in the field, although the skin damage is somewhat more irregular than was simulated here. Specimen 1E showed a significant 20% degradation in the lift-curve slope relative to the undamaged specimen, with

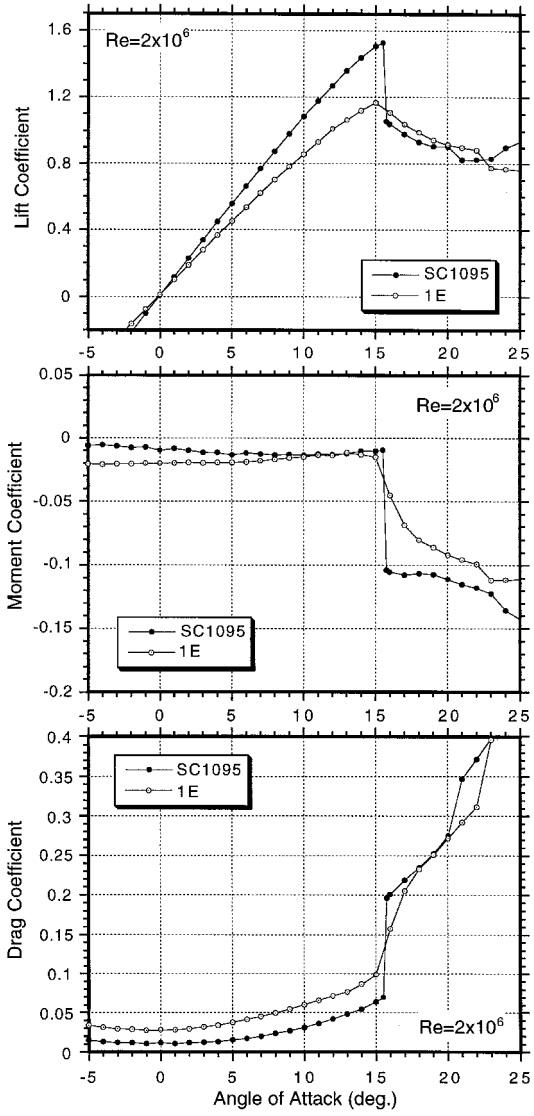

Fig. 7 Comparison of the lift, moment, and drag coefficients of specimen 1E (mid-span hole) vs the undamaged SC1095 section.

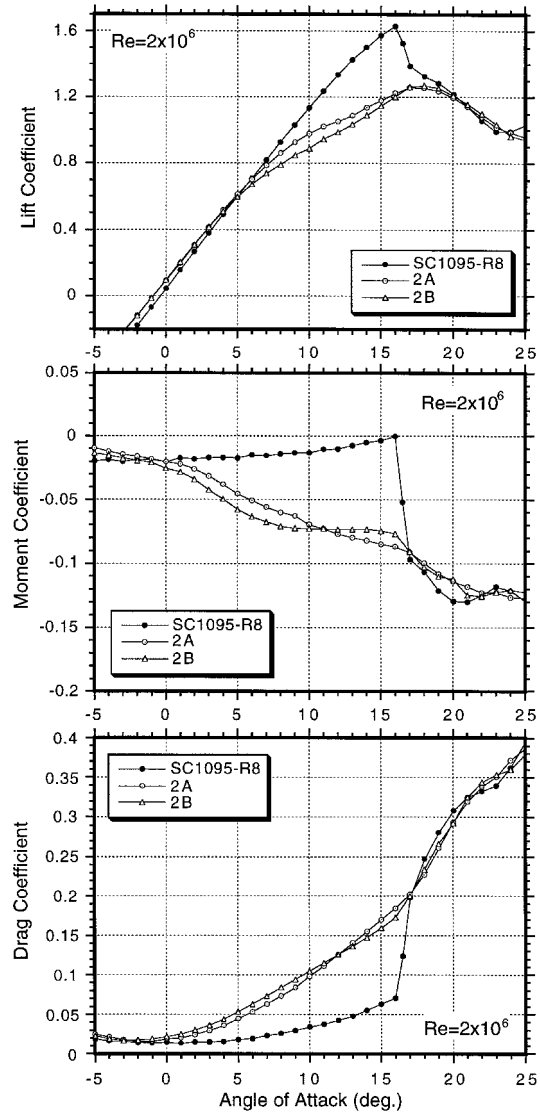

Fig. 8 Comparison of the lift, moment, and drag coefficients of specimens 2A (leading-edge hole) and 2B (leading-edge hole with simulated petalling) vs the undamaged SC1095-R8 section.

little change in the zero-lift angle of attack. The maximum lift coefficient was degraded by about 0.35, which was larger than that found for the previous specimens. The pitching moment appeared to be only slightly affected by this form of damage, with a small nose-up change in the zero-lift moment and a slight aft movement of the c.p. at lower angles of attack. The nonlinear behavior of the moment prior to the stall and moment break is symptomatic of the development of the vortical flow structure documented previously in Fig. 2b. A notable drag penalty was also realized with specimen 1E, with the zero-lift drag coefficient being about 0.028 compared to the undamaged value of 0.011. This increment, however, increased somewhat with increasing angle of attack, which is a result of the progressive intensification of the vortical flow structure documented previously by flow visualization. The lift-to-drag ratio for this damaged specimen was very severely degraded relative to the undamaged section, with the maximum lift-to-drag ratio being only about 15.

Figure 8 shows a comparison of the results obtained from specimens 2A and 2B (circular hole at the leading edge through the metal spar) relative to the undamaged SC1095-R8 specimen. Specimen 2B differed from specimen 2A by the addition of a series of serrations around the upper surface lip of the leading-edge hole. This represented the petalling effect that is usually associated with the penetration of a metal spar or skin by a ballistic projectile fired from below the rotor. Of interest in this case is that at the low negative angles of attack the lift was relatively unaffected compared with the undamaged specimen. The lift increased in a linear manner until an angle of attack of about 6 deg, where there was a sudden decrease in the lift-curve slope. As a result the maximum lift coefficient of this specimen was found to be degraded by nearly 0.4 relative to the undamaged specimen. However, like specimen 1B, the maximum lift was obtained at a higher angle of attack, in this case about 2–3 deg higher. This is a direct result of the vortical flow development from the damaged region (cf., Fig. 2d), which tended to maintain the lift (albeit at a reduced value compared to the undamaged specimen) to much higher angles of attack.

Because of the formation of the vortical flow over the chord, the pitching moment and drag of specimens 2A and 2B were found to quickly diverge as the angle of attack was increased beyond 0 deg. The aft movement of the c.p. is, again, a result of the vortical flow structure that trails over the blade. Note from Fig. 8 that the growth in the drag coefficient for specimens 2A and 2B were continuous but extremely rapid, and built to a value in excess of 0.2 prior to the final gross breakdown of the flow structure at about 18-deg angle of attack. In the normal operational angle-of-attack range, a substantially

higher drag was realized than for any of the other sections. Much of this drag arose from the vortical flow structure generated at the leading-edge lip of the hole.

Figure 8 also shows that the effects of the serations (petalling) were small. There was a slight degradation in the lift over specimen 2A between angles of attack of 6 and 18 deg. As noted previously, while the maximum lift of these sections was significantly degraded by the damage, the angle of attack for maximum lift was 3 deg higher at about 18 deg. The pitching moment for specimen 2B showed some deviations relative to specimen 2A, suggesting that the serrations had some effect on the chordwise pressure distribution, although they were minor. Figure 8 also shows that the addition of serrations increase the section drag by a maximum of 10–15%. Overall, it appeared that the hole was the source of most of the aerodynamic degradation relative to the undamaged section, the serrations or petalling producing only a minor further degradation in aerodynamic performance.

Finally, Fig. 9 shows a comparison between specimen 2C (circular hole in the trailing edge) and the undamaged specimen with the SC1095-R8 section. This damage configuration was the same as that used for specimen 1A, the main objective here being to examine the effects of the same amount of damage on the two different airfoil sections. The effects of damage at the trailing edge were previously found for the SC1095 airfoil (specimen 1A) to be relatively mild (see Fig. 4) and the same was found true for the SC1095-R8 section. The effects on the lift-curve slope and zero-lift angle were found small, with a negligible decrease in maximum lift coefficient. However, in this case the maximum lift was obtained at a higher angle of attack than for the undamaged section. It can be clearly seen from Fig. 9 that leading-edge damage does, in fact, delay the onset of the drag rise associated with gross flow separation and stall by about 1.5 deg. A slightly more rounding of the lift curve prior to maximum lift suggested that the damage promoted separation at lower angles of attack, and this can be correlated with the vortical flow development noted previously in Fig. 2f. The pitching moment curve showed that trailing-edge damage moved the aerodynamic center slightly forward. The effects of this form of damage on the drag were small and of the same order as for specimen 1A (SC-1095 airfoil).

Pressure Distributions

Chordwise and spanwise pressure measurements were mainly created to assess the three-dimensional nature of the airloads in the damaged regions. These measurements are important for assessing and understanding the local effects of damage and for helping to validate computational models of the flowfield. However, part of the study was also to address

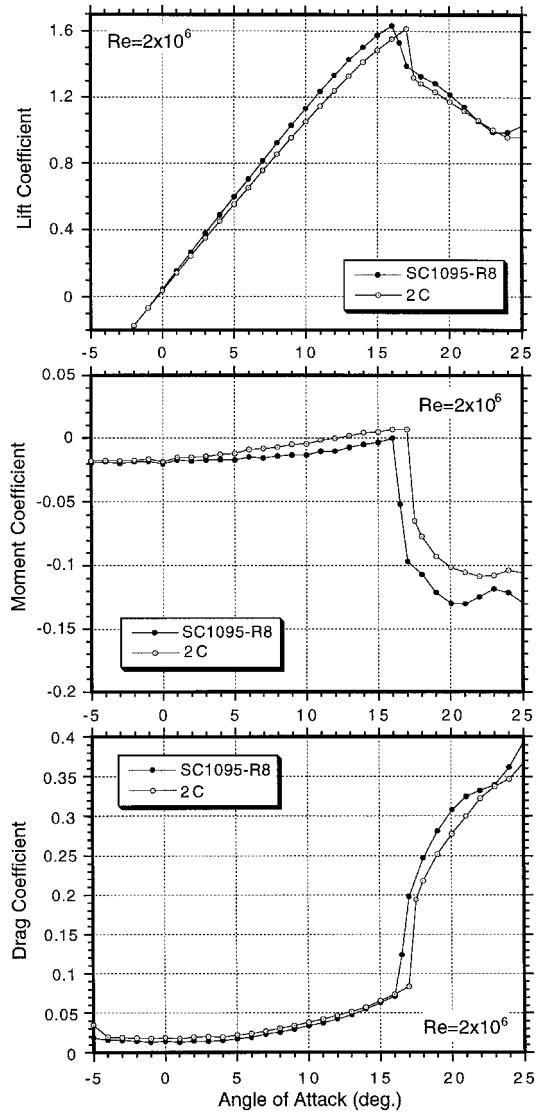

Fig. 9 Comparison of the lift, moment, and drag coefficients of specimen 2C (trailing-edge hole) vs the undamaged SC1095-R8 section.

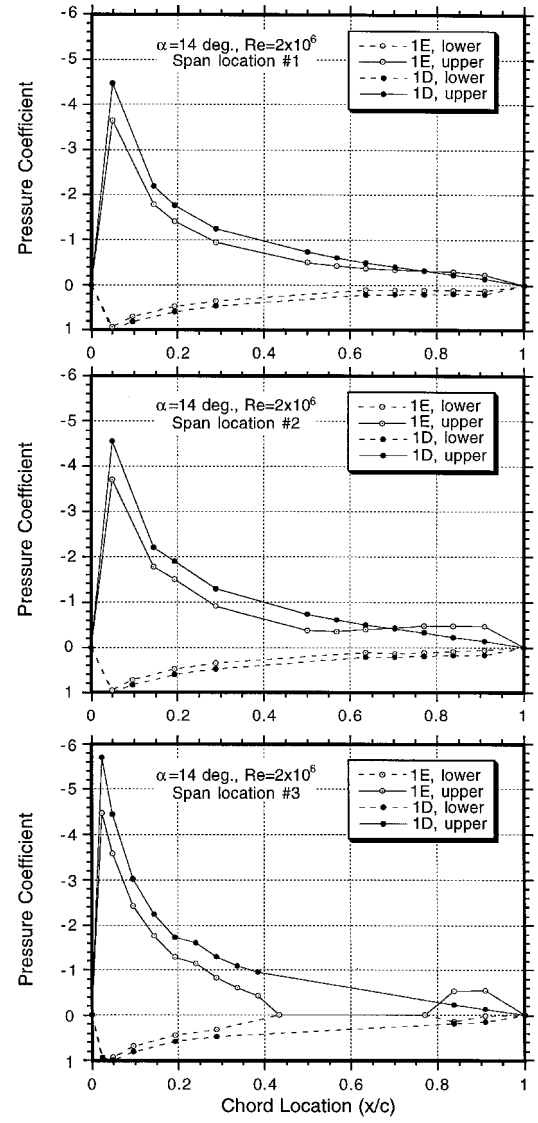

Fig. 10 Comparison of chordwise pressure distributions on specimens 1D and 1E at an angle of attack of 14 deg.

the uncertainties in force balance results vs integrated chordwise pressures. For the undamaged specimens, the results of sectional pressure integration for the lift were found to correlate well with the force balance measurements.[15] No comparisons of the pitching moment or pressure drag were made because of the relatively low number of pressure taps.

Figure 10 shows typical results for the chordwise pressure distributions measured on the undamaged and damaged (1D vs 1E) specimens at each of the three spanwise locations defined previously. These operating conditions were close to maximum lift. It was clear from the pressure distributions that trailing-edge separation had become established over almost the entire span of the blade. At the outer span location (no. 1), the separation point had only migrated forward to about 85% chord. This was confirmed by the flow visualization shown in Fig. 2b. With any further increase in angle of attack the blade specimens were found to stall. These results basically confirm the flow-visualization results in that the flow separation on the specimens is mostly confined to regions downstream and in the immediate vicinity of the damaged region.

Conclusions

An experimental study was conducted about the aerodynamic effects of ballistic damage on helicopter airfoil sections. In most cases the overall aerodynamic characteristics of the damaged sections were found to be degraded relative to their respective undamaged sections. The severity of this degradation generally increased as the damaged area was located closer to the leading edge, as well as by increasing size of the damaged area. In general, the lift-curve slope was found to decrease by varying amounts depending on the chordwise location and extent of damage. For the representative damage imposed in this study the sectional drag was increased up to four times that of the drag of the undamaged airfoils. Damage caused the aerodynamic center location to move slightly forward or aft, depending on the chordwise position of the damage. Flow separation was found to be initiated at the upstream leading edge of the damaged regions, followed by a growth in separation, both in span and intensity, with increasing angle of attack. Some damaged regions were found to produce a pair of counter-rotating vortices. This phenomenon tended to maintain the lift coefficients on the damaged section, but with much larger drag and aft movement of the c.p. For the specimens tested, the airfoil shape was found to play only a minor role in the resulting aerodynamic degradation from damage.

Acknowledgments

This work was sponsored by the U.S. Army Research Laboratory at Aberdeen Proving Ground, Maryland, under Contract DAAL01-94K-0084. Ki C. Kim of the Air Systems Branch was the Technical Monitor. The authors would like to acknowledge the assistance of Erwin Moedersheim, Andrew Baker, Ming Zhang, Ashish Bagai, Jewel Barlow, Robert Wozniack, Kenneth Kueny, and Charles Lessig for their contributions to this work.

References

[1]Foulk, J. B., "Survivability of the Army/Sikorsky YUH-60A Helicopter," 32nd Annual National V/STOL Forum of the American Helicopter Society, Washington, DC, May 1976.

[2]Atkinson, D. B., and Ball, R. E., "A History of the Survivability Design of Military Aircraft," AIAA Paper 95-1421, April 1995.

[3]O'Bryon, J. F., "The Difficult Task of Striking a Balance Between Testing and Modeling and Simulation: The Live Fire Test Case," *National Defense Magazine*, Feb. 1997.

[4]O'Bryon, J. F., "Live Fire Testing: The Legislation and It's Impact," *US Army (RDA) Magazine*, May/June 1987, pp. 1–3.

[5]Zinberg, H., Johnson, J., and Reddick, H., "The Survivability of Helicopters to Rotor Blade Ballistic Damage," American Helicopter Society/NASA Ames Conference on Helicopters Structures Technology, Nov. 1977.

[6]Anon., "Effects of Machine Gun and Cannon Fire on the Lift and Drag Properties of Airplane Wings," Rept. for Ballistic Research Labs., Aberdeen Proving Ground, by NASA Langley Research Center, Hampton, VA, June 1936.

[7]Biot, M. A., and Arnold, L., "Study of Vulnerability of Aircraft to Damage Induced Flutter," Ballistic Research Labs., Aberdeen Proving Ground, Rept. 743, Oct. 1950.

[8]Reece, J. W., "Interpretation of the Drag Changes Measured in the Wind Tunnel Tests of a Holed Wing," Cornell Aeronautical Lab., Inc., Rept. G1-634-G-1, March 1952.

[9]Chang, J. H., and Stearman, R. O., "The Effects of Warhead-Induced Damage on the Aeroelastic Characteristics of Lifting Surfaces," *Aeroelastic Effects*, Vol. 1, U.S. Air Force Office of Scientific Research, TR-80-1039 (N81-13955), 1980.

[10]Westkaemper, J. C., and Chandrasekharan, R. M., "The Effects of Warhead-Induced Damage on the Aeroelastic Characteristics of Lifting Surfaces," *Aerodynamic Effects*, Vol. 2, U.S. Office of Scientific Research, TR-80-1040 (N81-17048), 1980.

[11]Eastman, L., "UH-60A Dynamic Main Rotor Blade Ballistic Vulnerability Assessment," United Technologies Sikorsky Aircraft, SER-701981, 1993.

[12]Leishman, J. G., "Aerodynamic Characteristics of a Helicopter Rotor Airfoil as Affected by Simulated Ballistic Damage," U.S. Army Research Lab., Rept. ARL-CR-66, April 1993.

[13]Rae, W. H., Jr., and Pope, A., *Low-Speed Wind Tunnel Testing*, 2nd Ed., Wiley, New York, 1984, pp. 93–95.

[14]Jepson, D, Moffitt, R., Helizinger, K., and Bissell, J., "Analysis and Correlation of Test Data from an Advanced Technology Rotor System," NASA CR 3714, Aug. 1983.

[15]Leishman, J. G., "Experimental Investigation into the Aerodynamic Characteristics of Helicopter Rotor Airfoils with Ballistic Damage," U.S. Army Research Lab. Rept., ARL-CR-295, April 1995.

[16]Robinson, K. W., "Aerodynamic Characteristics of Rotor Airfoils as Affected by Simulated Ballistic Damage," M.S. Thesis, Univ. of Maryland, College Park, MD, May 1995.

[17]Robinson, K. W., and Leishman, J. G. "The Effects of Ballistic Damage on the Aerodynamics of Helicopter Rotor Airfoils," *Proceedings of the American Helicopter Society 53rd Annual Forum* (Virginia Beach, VA), American Helicopter Society, Alexandria, VA, 1997.